Numerical optimization of the EFP charge based on an MPB mine

Dariusz Pyka[1]

[1] *Wroclaw University of Science and Technology, Faculty of Mechanical Engineering, Department of Mechanics,*
Materials Science and Engineering, 25 Smoluchowskiego Street, 50-372 Wroclaw, Poland, https://orcid.org/0000-0002-9509-354X

Abstract

This article presents a numerical optimization of an explosively formed charge insert based on an anti-bullet, anti-tank MPB mine (*pl. mina przeciwburtowa, eng. anti-side mine*). For this purpose, first of all, the chemical composition and microstructure of the currently used EFP inserts and the target material - armour-piercing steel - were analyzed. Then, a series of numerical analyses were carried out, during which not only the material of the EFP insert was changed, but also its thickness, in terms of the most efficient combination, i.e. the initial speed during forming, but also the penetration ability of the insert. The Johnson-Cook constitutive strength model was used to describe the behaviour of materials in the computational environment, and the Jones-Wilkins-Lee model was used to describe the pressure during a detonation. To describe the formation of the EFP charge, SPH particle hydrodynamics was used, which the author had developed in his previous works, thanks to which it was possible to efficiently describe the highly dynamic process. The last element of the research was the validation of numerical models carried out at a military training ground during an experimental study. The results obtained as a result of numerical analyses allowed for the determination of the most optimal combination of material and insert thickness, which indicated future directions of development in order to improve solutions in the field of anti-tank EFP.

1. Introduction

For over a dozen years, anti-tank mines have been a special type of sapper ammunition that allows for the effective destruction of tanks, armoured personnel carriers and other vehicles in a horizontal plane from a distance of up to 200 meters (**Motyl et al., 2017; Laine et al., 2002**). In practice, however, effectiveness in diverse terrain (e.g. hilly or covered with vegetation) is limited to 50 meters (**Held, 2009**). Depending on the terrain conditions, i.e. the possibility of the full use of the anti-bullet mine's striking range, it can replace about 10 classic anti-tank mines in terms of effectiveness (**Kurzawa rt al., 2018; Śliwiński, 2011**).

Modern anti-bullet mines are manually installed in places where the use of anti-track and anti-bottom mines is difficult or ineffective (e.g. where they are easy to detect and neutralize) (**Krzystała et al., 2023**). They are also used to increase the effectiveness of traditional mine barriers (**Baur, 2024; Szczepaniak et al., 2019**). Thanks to their tactical and technical properties, anti-bullet mines are particularly useful for quickly blocking and securing

various types of roads, built-up areas and places of anticipated movement and regrouping of enemy troops, such as water obstacles, passes, valleys, and passages in forest complexes. They can also be used to temporarily close passages in existing mine barriers or defend them (**Graswald et al., 2019; Morrison et al., 2007**).

Previous achievements in the field of numerical research were mostly based on the standard FEM method (**Li et al., 2009; Cardoso and Teixeira-Dias, 2016**). This is related to the use of appropriate constitutive models and the setting of appropriate initial boundary conditions. In the case of detonation research and simultaneously conducted numerical simulations, it is important to describe the appropriate space (air domain) in which the detonation is initiated and the associated sudden change in pressure occurs. For this purpose, the Johnes-Wilkins-Lee equation of state is most often used, most often also combined with the Mie-Gruneisen model describing the initial pressure of the system (**ABAQUS, 2009; Micallef et al., 2015**). Numerical research in the literature related to the analysis of detonation is often carried out using hydrodynamic particles (SPH) (**Zhang et al., 2013; Du et al., 2016**), but so far EFP detonation have been modelled using standard FEM methods (**Wu et al., 2007**). Often, high deformations of individual finite elements in a highly dy-

Corresponding author: Dariusz Pyka
e-mail address: dariusz.pyka@pwr.edu.pl

namic impact process constitute a big problem in numerical problems. The approach described earlier mainly concerns the approach to modelling the detonation itself. There are also many methods for modelling the cover itself in literature. This is related to the use of standard FEM, SPH and the combination of these two methods, i.e. the use of the so-called hybrid FEM, where the projectile is modelled using standard FEM and the shield is modelled using SPH particles (**Roszak et al., 2023; Göçmen et al., 2022**). Regardless of the approach used, it is also necessary to use appropriate constitutive models describing the behaviour of individual materials. In this case, the choice of model largely depends on the strength characteristics of the material, including the use of elements responsible for the rate of deformation and thermal softening. Detonations are very dynamic phenomena compared to, for example, firing a bullet from a rifle, where velocities reach approximately 2000-3000 m/s in the case of EFP explosively formed charges. It should also be remembered that in the event of a detonation, the influence of temperature on the behaviour of the material is often significant. In this context, many models are widely used. The most popular model describing the behaviour of metallic materials is the Johnson-Cook model and the related Johnson-Cook damage model (**Li et al., 2023; Wiśniewski and Tomaszewski, 2011; Flores-Johnson et al., 2014**). The model parameters are relatively easy to determine, and the model itself takes into account both the influence of strain rate and the influence of thermal softening.

The aim of this work is to optimize inserts in explosively formed charges (EFP), while analyzing the accuracy of the applied numerical methods. In his previous works, the author focused on modelling phenomena using SPH particles, including in the context of charge formation analysis (**Pyka et al., 2020**). Previous preliminary research has confirmed that the use of the above-mentioned method allows for reliable mapping of the bullet impact process in the shield, while maintaining continuity in the formation of the charge without excessive deformation of the finite elements, which is a novelty in the context of modelling the formation of EFP inserts using the SPH particle method.

2. Materials and methods

2.1. Tested object

The object examined in this work is a Polish off-route anti-tank mine – the MPB mine (see **Figure 1**). The MPB anti-bullet mine equipped with an EFP charge was introduced into the equipment of the engineering forces of the Polish Army. It is tactical and technical parameters are comparable to other mines of this type used in the world. This mine was developed by the Military Institute of Engineering Technology in cooperation with Bydgoszcz Electronic Plants "BELMA" S.A. and the Military University of Technology. In the MPB-ZN ver-

Figure 1: MPB Mine at military training ground

sion, the detonation is triggered by a non-contact detonator activated by an acoustic sensor, in the MBP-ZK version by a mechanical-electric contact detonator. The armour-damaging element is an explosively formed projectile. The mine also destroys vehicles protected by reactive armour. The mine parameters are presented in the table below (see **Table 1**).

2.2. Microscopic analyses

An example of the microstructure of a copper mine liner material is shown in **Figure 2**. The images were prepared using a microscope Nikon Eclipse MA 200 light microscope, magnification: 200x.

On the surfaces of the through-hole formed in the plate after destruction, a layer of clump material, irregular in thickness, was formed (see **Figure 3**). Observations conducted on metallographic scrapings made in a cross-section to the surface showed that fragmentation of the plating occurred during the passage and numerous fragments of the plate material are visible on the surface (see **Figure 3a**). In addition, there are cracks in the near-surface zone formed after the passage of the clump. During the observation, it was revealed that the Cu clump material is strongly adhesively bonded to the surface of the steel plate and forms an irregular coating on its surface with considerable porosity. The outer surface of the coating shows considerable irregularity with numerous pits and detached fragments (see **Figure 3b**). It should be noted that the detached fragments of the plate residing on the surface of the formed hole in whole or in part are also coated with a layer of clump material.

2.3. Ballistic test

The tests were carried out at a military training ground. An explosively formed charge was fired from a

Technical data of MPB mines					
Mass [kg]	Length [mm]	Height [mm]	Width [mm]	Load type [-]	RHA penetration ability [mm]
45	450	700	390	Cumulative EFP	100
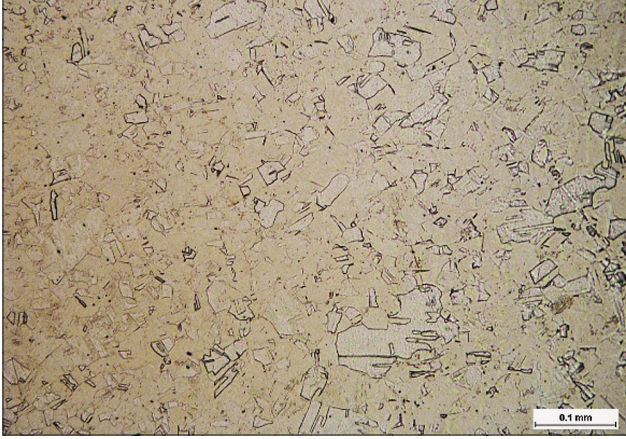
Figure 2: Microstructure view of the base material of the insert taken from the MPB mine

distance of 50 m from the target. The shelling was carried out three times. The target was a plate made of Armox 370T steel with dimensions of 1.5 m × 1.0 m × 0.1 m and a mass of approximately 1,200 kg. A photo of the test stand at the training ground is shown below (see **Figure 4**). Atmospheric conditions during the test: 21°C, no wind, cloudy. The aim of the research was to assess the penetration capabilities of a charge fired from a distance of 50 m against sheet metal corresponding to the thickness of the tank's armour.

2.4. Preparation of numerical model

To describe the behaviour of elastic-plastic materials, the Johnson-Cook constitutive model (1) was used togeth-

er with the failure model (2) for the sample material. This model is very often used due to the relatively low complexity of determining material constants and its availability in many computing environments (**ABAQUS, 2009; Grygier et al., 2024; Burley et al., 2018**).

$$\sigma = \left(A + B\varepsilon^n\right) \cdot \left[1 + Cln\left(\frac{\dot{\varepsilon}}{\dot{\varepsilon}_0}\right)\right] \cdot \left[1 - \left(\left(\frac{T - T_0}{T_m - T_0}\right)^m\right] \quad (1)$$

$$\varepsilon^f = \left(D_1 + D_2 \exp D_3 \sigma^*\right) \cdot \left[1 + D_4 \ln\left(\frac{\dot{\varepsilon}}{\dot{\varepsilon}_0}\right)\right] \cdot \left[1 - D_5\left(\frac{T - T_0}{T_m - T_0}\right)^m\right] \quad (2)$$

Where:

A, B, C, n, m – the J-C material behaviour coefficients,

ε – is the plastic strain,

$\dot{\varepsilon}$ – the plastic strain rate,

$\dot{\varepsilon}_0$ – the reference strain rate,

T – the current temperature,

T0 – the room temperature,

Tm – the melting temperature,

D1, D2, D3, D4 and D5 – the input constants determined empirically,

ε^f – the plastic strain to fracture,

σ^* – the equivalent stress.

The SPH method described by the Lagrange equations is a mesh-free method, therefore very efficient for high-speed dynamic simulations. This method includes two approximation steps. In the first one – kernel approximation –described with a function (3).
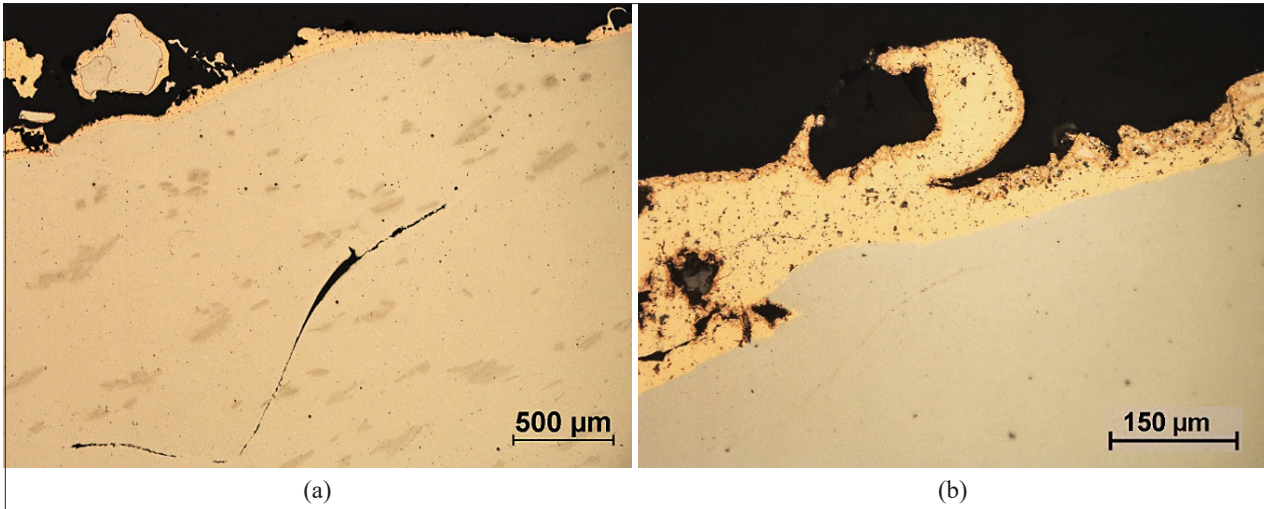

Figure 3: Cross-sectional view of the steel plate material to the surface of the formed through-hole:
(a) fragmentation of the material, the inner crack of the plate with the revealed coating of the clump material on the surface,
(b) the structure of the clump material formed on the surface of the plate.

$$\left(f\left(x \right) \right) = \int_{\Omega} f\left(x' \right) W\left(x - x', h \right) dx' \quad (3)$$

Where:

$(f(x))$ – the approximated value,
W – the smoothing function representing,
h – the smooth length,
x – the position vector of the particle.

In the second step - particle approximation – the field function and its derivative are approximated as a weighted sum over the surrounding particles in the carrier domain (**Zhang et al., 2021; Liu and Liu, 2023**).

The Mie-Gruneisen equation (4) was used to describe air pressure in the simulation space (**ABAQUS, 2009**).
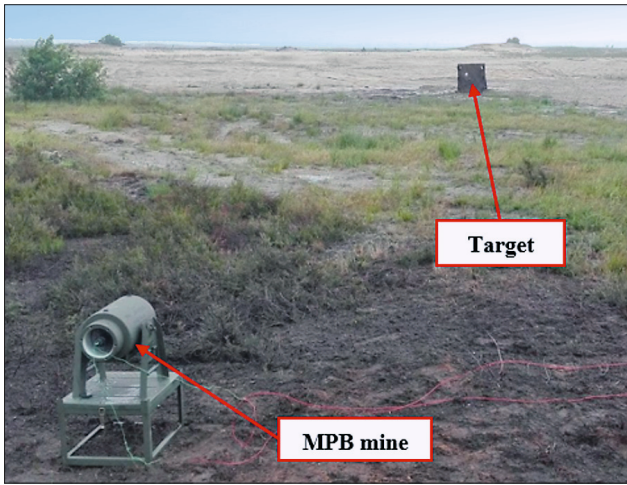
Figure 4: Research station at a military training ground

$$P = p_0 + \gamma \rho_a E_0 \quad (4)$$

Where:

p0 – the initial air pressure;
ρa – the density of air;
γ – the Gruneisen coefficient;
E0 – the initial internal energy.

The behaviour of gunpowder and gunpowder gases is described using the equation of state. The most commonly used equation of state for detonation calculations is JWL (Jones-Wilkins-Lee), which allows you to determine the pressure (5) (**ABAQUS, 2009; Baranowski et al., 2020**).

$$p = A^* \left(1 - \frac{\omega \eta}{R_1} \right) \exp^{\frac{-R_1}{\eta}} + B^* \left(1 - \frac{\omega \eta}{R_2} \right) \exp^{\frac{-R_2}{\eta}} + \omega \rho_{pd} \quad (5)$$

Where:

η – is the ratio of the density,
ρ – of detonation products to the initial density,
$\rho 0$ – of the original explosive,
A*, B*, R1, R2 and ω – the fitting coefficients obtained from experiments,
κpd – the pre-detonation bulk modulus.

The material parameters used for the simulations are listed in the table below (see **Table 2**).

According to the manufacturer's data, the charge is a combination of Hexogen and TNT in 60/40 proportions. In numerical simulations, the TNT equivalent was adopted and the parameters were scaled appropriately. The detonation point was determined as the beginning of

Table 2: Material constants used for numerical simulations (**Panowicz and Konarzewski, 2020; Kurzawa et al., 2018; Xu et al., 2019, Sliwinski et al., 2016; Mehreganian et al., 2018; Nsiampa et al., 2009**)

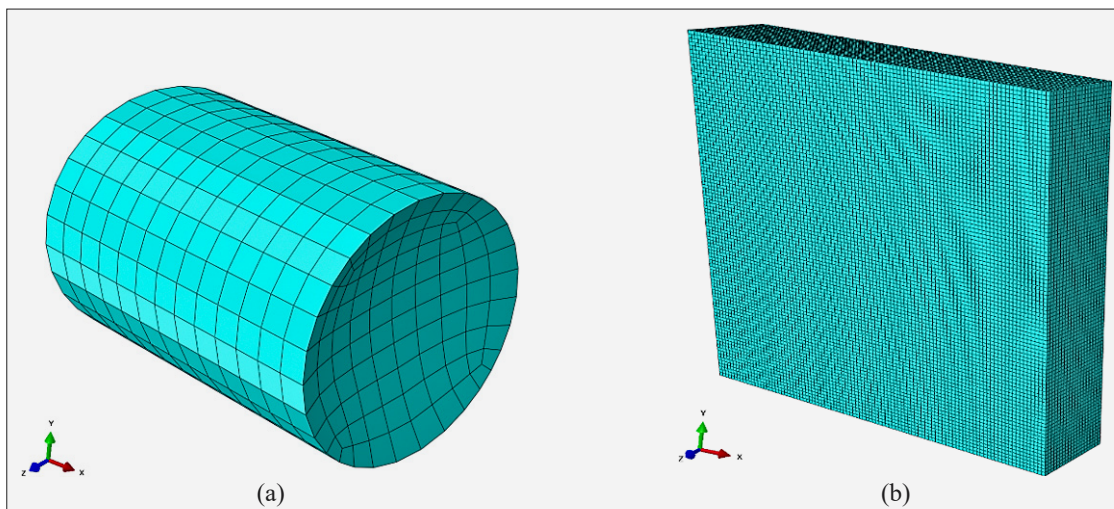| Explosive										
TNT	ρ^*	D	P_{CJ}	A^*	B^*	R_1	R_2	ω	κ_{pd}	Source
	[kg/m³]	[m/s]	[GPa]	[GPa]	[GPa]	[-]	[-]	[-]	[GPa]	
	1730	8193	28.00	609.00	13.00	4.50	1.40	0.25	9.00	(**Pyka et al., 2020**)
Liner material										
	ρ	E	ν	A	B	C	n	m		Source
	[kg/m³]	[GPa]	[-]	[MPa]	[MPa]	[-]	[-]	[-]		
Cooper	8960	128	0.36	80	500	-	0.605	1.00		(**Panowicz and Konarzewski, 2020**)
AC-44200	2730	70	0.33	110	330	0.008	0.100	1.00		(**Kurzawa et al., 2018**)
S355	7820	210	0.35	807	1660	0.008	0.100	1.00		(**Xu et al., 2019**)
Armco	7800	210	0.37	233	460	0.047	0.320	0.55		(**Sliwinski et al., 2016**)
Lead	11300	115	0.42	24	40	0.010	0.500	1.00		(**Sliwinski et al., 2016**)
Armour steel										
	ρ	E	ν	A	B	C	n	m		Source
	[kg/m³]	[GPa]	[-]	[MPa]	[MPa]	[-]	[-]	[-]		
A370T	7900	210.00	0.30	1150	838	0.076	0.283	-		(**Mehreganian et al., 2018**)
	D_1 [-]		D_2 [-]		D_3 [-]		D_4 [-]		D_5 [-]	
A370T	0.17		0.034		-2.44		-0.05		-		(**Nsiampa et al., 2009**)

Figure 5: Discretized elements of numerical simulations: (a) TNT, (b) discretized sample.

the contemporary system (0,0,0) with the detonation initiation equal to 0 s. The modelling of the explosive charge using the FEM and SPH methods for 3 selected discretization element sizes was chosen as a comparative basis. Puncture modelling of a 100 mm thick Armox 370T steel plate was performed using the Abaqus/Explicit program. Abaqus/Explicit is a powerful finite element analysis (FEA) software specifically designed for solving highly nonlinear and transient dynamic prob-

lems, often involving large deformations, complex material behaviours, and high-speed events. For this purpose, modelling the formation of an EFP mine based on an MPB mine. With a copper insert, which is confirmed by tests of the microstructure of the sampled material. In order to verify the penetration of the armour plate, simulations of hitting a copper slug into the armour plate were performed. For this purpose, sections of armour plate with dimensions of 500×500×100 mm were per-
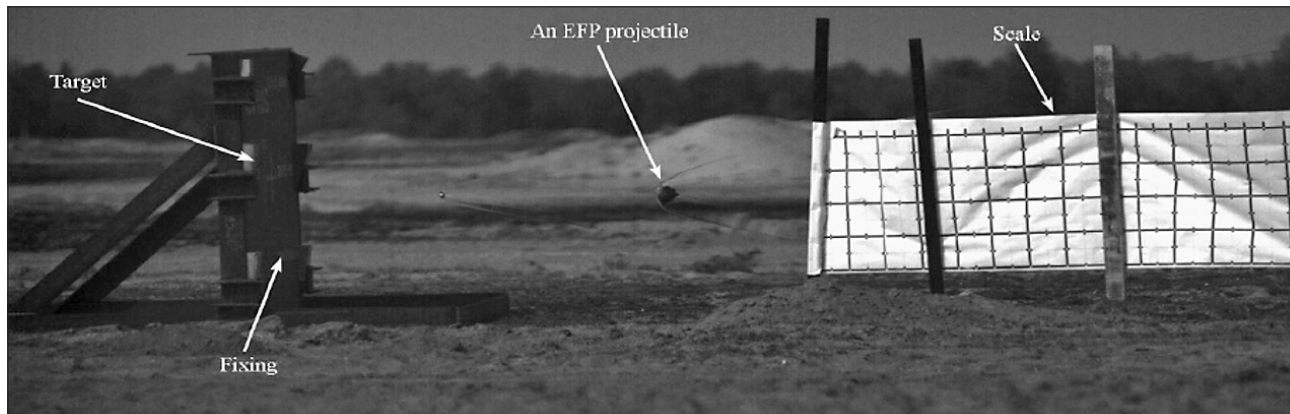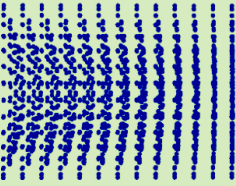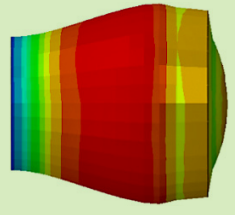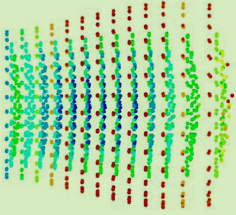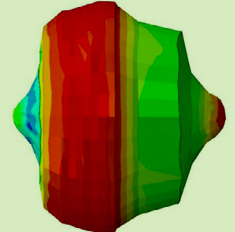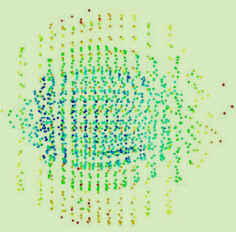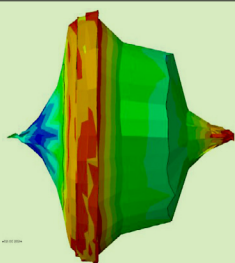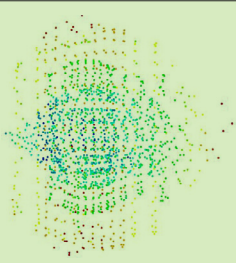

Figure 6: Flying projectile at military training ground (**Śliwiński, 2011**)

Figure 7: EFP projectile hitting target (**Kurzawa et al., 2018**)

Table 3: Comparison of explosive charge formation for two different simulation methods

Time [ms]	FEM	SPH
0		
0.5		
1.5		
2.5		

formed. The size of the Hex element was 3.0 mm. The individual elements of the system are presented below (see **Figure 5**).

The MPB mine charge was optimized by changing the geometry of the insert and the material used. The base radius was R = 300 mm, and three insert thicknesses were selected: 5, 10, 15 mm, respectively.

3. Results

3.1. Results of ballistics tests

In the experiment conducted, a schematic diagram of which is shown in **Figure 6**, the detonation lead to the perforation of the slab by means of an explosively formed projectile (EFP). The impact of the slug projectile on the slab resulted in the perforation of a piece of material with a cylindrical shape, with an elliptical base of 121 mm and 128 mm. Reduction of the initial thickness of the slab, which was 100 mm, was caused by damage to the material resulting from the hydrodynamic impact of the projectile on the front surface of the plate. The outer surface of the fragment was curved and rounded in the direction of the impact forces, with clearly visible cracks in the central part of the structure.

The process of hydrodynamic penetration of an explosively formed projectile (EFP) into steel armour can be described as a complex interaction between the projectile and the target material, where dynamic and thermomechanical phenomena play a major role. When the EFP strikes the steel armour at extremely high velocity, the kinetic energy of the projectile is concentrated on a small contact area, leading to a rapid increase in pressure in the impact zone (see **Figure 7**). As a result of this pressure increase, the projectile material and armour material begin to behave like highly viscous liquids, despite being solids. This state, referred to as hydrodynamic flow, is crucial to the penetration process. Under the influence of pressure and temperature, the armour material becomes locally plasticized, and is then pushed sideways or moves along the axis of the projectile, allowing it to penetrate
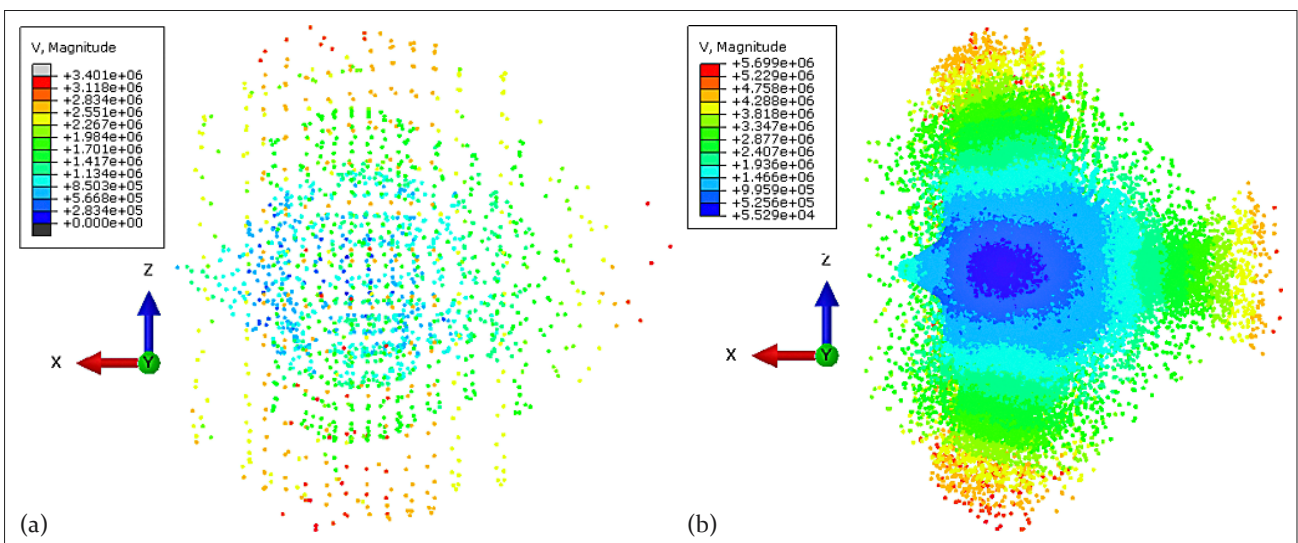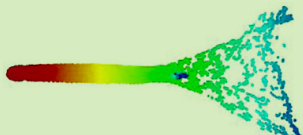

(a)

(b)

Figure 8: Comparison of explosive forming: (a) finite element size of 30 mm, (b) finite element size of 5 mm

Table 4: Slug formation for different materials and thickness of 5 mm

Material	Slug shape	Velocity [m/s]
Al-44200		3023
Armco		2250
Lead		2462
S355		2378
Copper		2418

Table 5: Slug formation for different materials and thickness of 10 mm
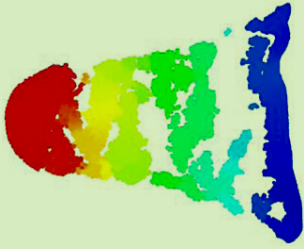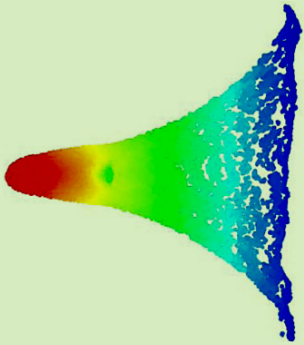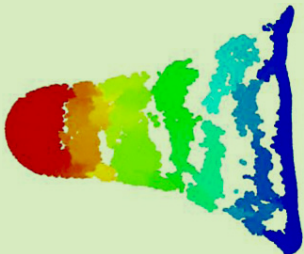
Material	Slug shape	Velocity [m/s]
Al-44200		2829
Armco		1876
Lead		1742
S355		1899
Copper		1765

further into the armour. This process is aided by the phenomenon of adiabatic heating, in which the energy of mechanical deformation is converted into heat, leading to further weakening of the material structure.

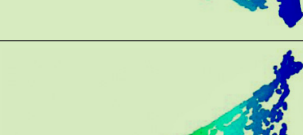### 3.2. Results of numerical analyses of the slug forming

The first differences were noticed in the process of forming the explosive charge. For standard FEM, the finite elements undergo significant deformation. This is not the case with SPH particles because they are not connected to each other by a mesh. A comparison of the explosive charge formation process for two simulation methods is presented below (see **Table 3**). The basic dimension of the finite element was 30 mm.

Additionally, a comparison of the influence of the finite element dimension on the form of the formed charge is presented below (see **Figure 8**).

Below (see **Tables 4-6**) is a summary of the slug formation speed up to 0.4 ms for various materials and geometric arrangements of the insert.

Depending on the material used and the thickness of the EFP insert, there are significant differences in both the speed and shape of the formed insert. In terms of the shape of the bullet being formed, lead is very advantageous in this case. The insert should not fragment or dis-

integrate during forming, which during the analyses indicates that a highly plastic lead is advantageously formed. Below (see **Figures 9–11**) a comparison of speeds depending on the material used and the thickness of the insert is also presented. The highest speeds were obtained for the smallest insert thickness, which is obviously due to the fact that they are the lightest. Interestingly, due to the lowest density of all selected materials, aluminium inserts achieve the highest speeds. Unlike other materials, the speeds of which do not differ that much. The lowest speed was obtained for the "heaviest" lead.

3.3. Results of numerical results for slug hitting the target

The process of piercing the cover is presented below (see **Table 7**).

Table 6: Slug formation for different materials and thickness of 15 mm

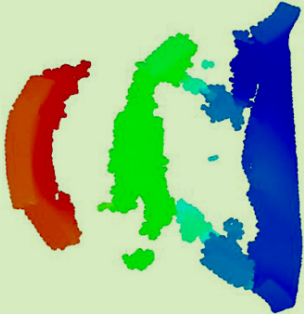| Material	Slug shape	Velocity [m/s]
Al-44200		2408
Armco		1466
Lead		1356
S355		1450
Copper		1372

Figure 9: Comparison of obtained projectile velocity for different materials and 5 mm EFP
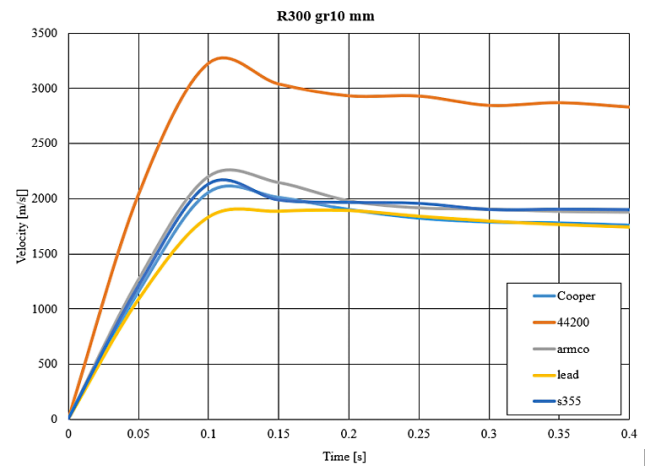
Figure 10: Comparison of obtained projectile velocity for different materials and 10 mm EFP insert
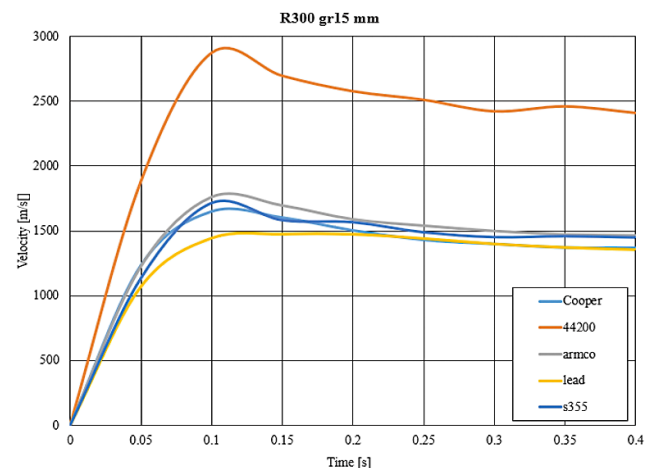
Figure 11: Comparison of obtained projectile velocity for different materials and 15 mm EFP insert

Numerical analysis using the particle hydrodynamics (SPH) method showed greater efficiency in modelling the formation process and impact of the EFP insert on the target, compared to the traditional finite element method (FEM). SPH better reflected the detonation mechanics, especially under conditions of extreme deformation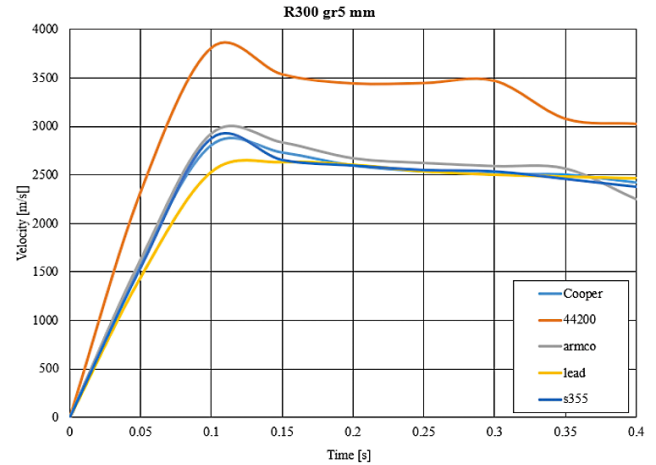. Experimental tests carried out on a military training ground confirmed the results of numerical analyses, demonstrating the effectiveness of the models used in predicting the behaviour of EFP inserts when hitting armour steel (see **Figure 12**).

Table 7: Sample destruction in a numerical environment

Time [ms]	Damage formation	Stress [MPa]
0.02		S, Mises (Avg: 75%) +8.422e+02 +7.720e+02 +7.018e+02 +6.316e+02 +5.614e+02 +4.913e+02 +4.211e+02 +3.509e+02 +2.807e+02 +2.105e+02 +1.404e+02 +7.018e+01 +0.000e+00
0.05		S, Mises (Avg: 75%) +1.258e+03 +1.153e+03 +1.048e+03 +9.434e+02 +8.386e+02 +7.338e+02 +6.289e+02 +5.241e+02 +4.193e+02 +3.145e+02 +2.097e+02 +1.048e+02 +7.936e-03
0.10		S, Mises (Avg: 75%) +1.258e+03 +1.153e+03 +1.048e+03 +9.434e+02 +8.386e+02 +7.338e+02 +6.289e+02 +5.241e+02 +4.193e+02 +3.145e+02 +2.097e+02 +1.048e+02 +7.936e-03

Table 8: Comparison of the results of the experiment with the simulation of the plate puncture

	Front	Back
Experiment	121 - 128 mm	110-115 mm
Numerical	105 - 111 mm	106-108 mm
Difference	13,3 - 15,2 %	3,7 - 6,1 %

EFP load. In the case of the experiment, this is due to the accuracy of execution. In numerical simulation, on the other hand, it is due to the de-scaling of components.

4. Conclusions

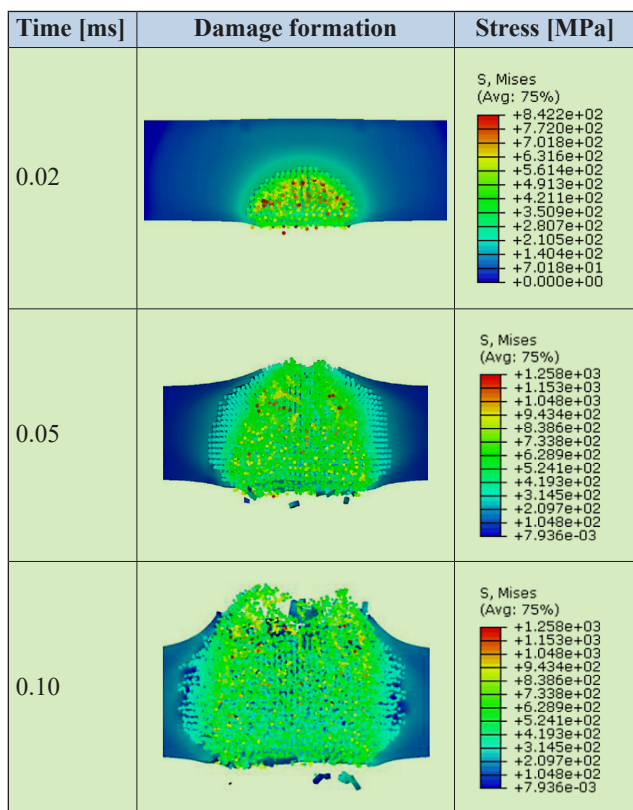This study presents a comprehensive numerical optimization of an explosively formed liner (EFP) used in anti-tank anti-bullet mines, specifically focusing on the MPB mine. The research included a detailed analysis of the chemical composition and microstructure of both the EFP inserts and the target material, which was anti-tank steel. Various material properties and thicknesses of EFP inserts were investigated through a series of numerical simulations to determine their impact on the initial forming speed and penetration capabilities.

The Johnson-Cook constitutive strength model was used to describe the behaviour of materials, and the Jones-Wilkins-Lee model was used to characterize pressure dynamics during a detonation. Particle hydrodynamics (SPH) was used to model EFP charge formation, building on previous developments in this methodology to effectively describe the highly dynamic process.

Experimental validation was carried out at a military training ground, which confirmed the accuracy of the numerical models. The tests included firing an Armox 370T

Above (see **Table 8**) is a comparison of the puncture of a 100-mm-thick steel plate made of Armox 370 T. The fit is below 15% regarding the front of the plate, while the discrepancies at the rear average around 4%, which represents a very good fit of the numerical model. Differences in the averages in both the experiment and the numerical simulation testify to the unsuitability of the
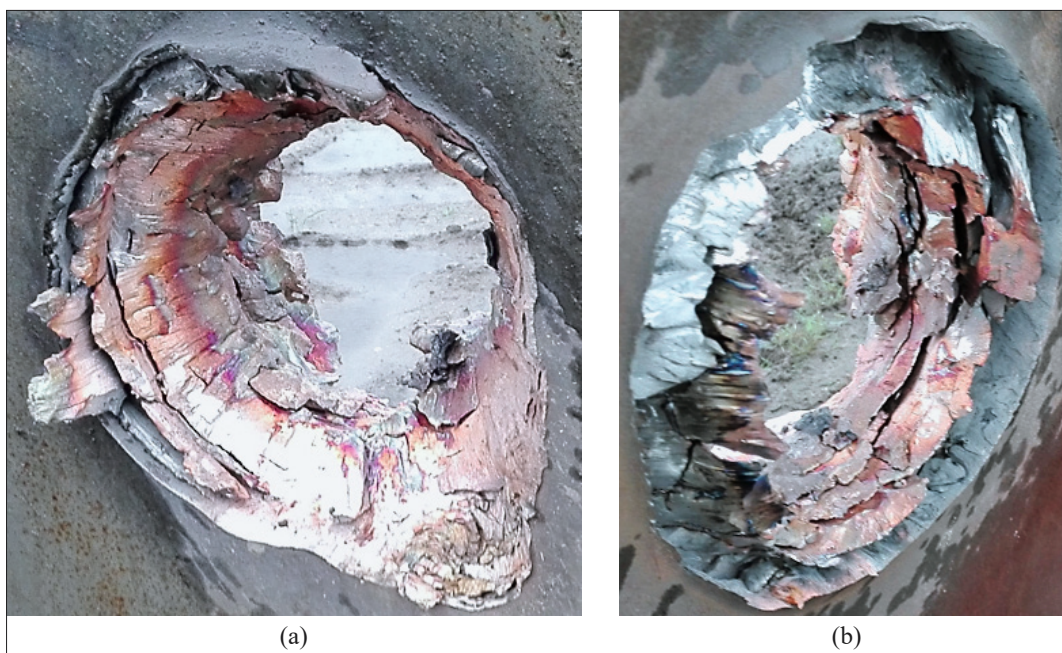

(a)   (b)

Figure 12: Puncture of the steel plate: (a) front, (b) back

steel plate, reproducing the conditions and dimensions of typical tank armour. The results highlighted the effectiveness of the SPH method compared to the traditional finite element method (FEM) due to its ability to handle extreme deformations without mesh entanglement.

The results of numerical analyses regarding the impact of an explosively formed insert (EFP) on a target showed significant differences depending on the insert material used and its thickness. The use of the EN-AC44200 aluminum alloy for the EFP insert allowed for the highest bullet speeds in all tested insert geometry variants.

In summary, the results of the numerical analyses indicate the need to optimize the thickness and material of the EFP insert in order to achieve the best combination of initial velocity and penetration ability. The identified optimal parameters constitute the basis for further development of anti-tank EFP insert technology, increasing the effectiveness of anti-bullet mines in various combat conditions. This research highlights the importance of integrating advanced numerical methods with experimental validation to develop effective military technology. Future focus should be on exploring additional insert materials and geometries to further increase the effectiveness of anti-bullet mines.

This work contributes to the development of armour-piercing munitions by offering a detailed analysis of material performance under explosive conditions and presenting a validated approach to optimizing EFP inserts.

Acknowledgement

6. References

Motyl, K., Magier, M., Borkowski, J. and Zygmunt, B. (2017): Theoretical and experimental research of anti-Tank kinetic penetrator ballistics. Bulletin of the Polish Academy of Sciences, Technical Sciences, 65, 399–404. https://doi.org/10.1515/bpasts-2017-0045

Laine, L., Ranestad, O., Sandvik, A. and Snekkevik, A. (2002): Numerical Simulation of Anti-tank Mine Detonations. AIP Conference Proceedings, 620(1), 431–434. https://doi.org/10.1063/1.1483570

Held, M. (2009): Anti-tank Mine Blast Effects. Journal of Battlefield Technology, 12(2), 1–7. Retrieved from https://doi.org/10.3316/informit.946822468852668

Kurzawa, A., Pyka, D., Bocian, M., Jamroziak, K. and Sliwinski, J: (2018). Metallographic analysis of piercing armor plate by explosively formed projectiles. Archives of Civil and Mechanical Engineering, 18(4), 1686–1697. https://doi.org/10.1016/j.acme.2018.06.006

Śliwiński, J: (2011). Protection of vehicles against mines. Journal of KONES Powertrain and Transport, 18(1), 565–572.

Krzystała, E., Sławski, S., Jarosz, T., Stolarczyk, A. and Polis M. Assessment of the human threat during the improvised explosive device detonation. 5th Polish Congress of Mechanics, 25th International Conference on Computer Methods in Mechanics, Gliwice 2023. Available online: https://content.pcm-cmm.com/abstracts/2_Biomechanics/259_Krzysta%C5%82a.pdf (accessed on 6 November 2023)

Baur, J. (2024): Ukraine is Riddled with Land Mines: Drones and AI Can Help. IEEE Spectrum, 61(5), 42–49. https://doi.org/10.1109/MSPEC.2024.10522930

Szczepaniak, M., Jasiński, W., Madej, W., Wojciechowski, A., Krysiak, P. and Śliwiński, J. (2019): Armoured Fighting Vehicle Destruction System. Problems of Mechatronics Armament Aviation Safety Engineering, 10(1), 135–142. https://doi.org/10.5604/01.3001.0013.0802

Graswald, M., Gutser, R., Breiner, J., Grabner, F., Lehmann, T. and Oelerich, A. (2019): Defeating Modern Armor and Protection Systems. https://doi.org/10.1115/HVIS2019-050

Morrison, J. J., Mahoney, P. F. and Hodgetts, T. (2007): Shaped Charges and Explosively Formed Penetrators: Background for Clinicians. BMJ Military Health, 153(3), 184–187. https://doi.org/10.1136/jramc-153-03-11

Li, X. J., Li, M. Z., Cai, Z. Y. and Sun, Y. M. (2009): Numerical simulation and experimental study on incremental forming of sheet metal. Cailiao Kexue Yu Gongyi/Material Science and Technology, 17(1), 66–69. https://doi.org/10.1038/s41598-024-67943-5

Cardoso, D. and Teixeira-Dias, F. (2016): Modelling the formation of explosively formed projectiles (EFP). International Journal of Impact Engineering, 93, 116–127. https://doi.org/10.1016/j.ijimpeng.2016.02.014

ABAQUS; Version 6.6; Analysis User's Manual Documentation; Washington University in St. Louis: St. Louis, MO, USA, 2009.

Micallef, K., Fallah, A. S., Pope, D. J., Moatamedi, M. and Louca, L. A. (2015). On dimensionless loading parameters for close-in blasts. International Journal of Multiphysics, 9(2), 171–193. https://doi.org/10.1260/1750-9548.9.2.171

Zhang, A., Yang, W.-S., Huang, C. and Ming, F. (2013): Numerical simulation of column charge underwater explosion based on SPH and BEM combination. Computers & Fluids, 71, 169–178. https://doi.org/10.1016/j.compfluid.2012.10.012

Du, Y., Ma, L., Zheng, J., Zhang, F. and Zhang, A. (2016): Coupled simulation of explosion-driven fracture of cylindrical shell using SPH-FEM method. International Journal of Pressure Vessels and Piping, 139–140, 28–35. https://doi.org/10.1016/j.ijpvp.2016.03.001

Wu, J., Liu, J. and Du, Y. (2007): Experimental and numerical study on the flight and penetration properties of explosively-formed projectile. International Journal of Impact Engineering, 34(7), 1147–1162. https://doi.org/10.1016/j.ijimpeng.2006.06.007

Roszak, M., Pyka, D., Bocian, M., Barsan, N., Dragašius, E. and Jamroziak, K. (2023): Multi-Layer Fabric Composites Combined with Non-Newtonian Shear Thickening in Ballistic Protection – Hybrid Numerical Methods and Ballis-

tic Tests. Polymers, 15(17). https://doi.org/10.3390/polym15173584

Göçmen, Y., Vural, H., Erdogan, C. and Yalçinkaya, T. (2022): Numerical analysis of ballistic impact through FE and SPH methods. Procedia Structural Integrity, 42, 1736–1743. https://doi.org/10.1016/j.prostr.2022.12.220

Li, L., Zhang, Y., Cui, X., Said, Z., Sharma, S., Liu, M., Gao, T., Zhou, Z., Wang, X. and Li, C. (2023): Mechanical behavior and modeling of grinding force: A comparative analysis. Journal of Manufacturing Processes, 102, 921–954. https://doi.org/10.1016/j.jmapro.2023.07.074

Wiśniewski, A. and Tomaszewski, Ł. (2011): Simulation of Steel Armour Penetration Using. Problems of Mechatronics Armament, Aviation, Safety Engineering, 4(6), 27–36.

Flores-Johnson, E. A., Shen, L., Guiamatsia, I. and Nguyen, G. D. (2014): Numerical investigation of the impact behaviour of bioinspired nacre-like aluminium composite plates. Composites Science and Technology, 96(May), 13–22. https://doi.org/10.1016/j.compscitech.2014.03.001

Pyka, D., Kurzawa, A., Bocian, M., Bajkowski, M., Magier, M., Sliwinski, J. and Jamroziak, K. (2020): Numerical and experimental studies of the Łk type shaped charge. Applied Sciences (Switzerland), 10(19), 1–20. https://doi.org/10.3390/app10196742

Wilewski, Supernowoczesna mina – sukces inżynierów, https://www.polska-zbrojna.pl/home/articleshow/5916 (accessed 14th March 2024)

Grygier, D., Kurzawa, A., Stachowicz, M., Krawiec, K., Stępczak, M., Roszak, M., Kazimierczak, M., Aniszewska, D. and Pyka, D. (2024): Investigations into the Material Characteristics of Selected Plastics Manufactured Using SLA-Type Additive Methods. Polymers, 16(11). https://doi.org/10.3390/polym16111607

Burley, M., Campbell, J. E., Dean, J. and Clyne, T. W. (2018): Johnson-Cook parameter evaluation from ballistic impact data via iterative FEM modelling. International Journal of Impact Engineering, 112, 180–192. https://doi.org/10.1016/j.ijimpeng.2017.10.012

Zhang, Z., Wang, C., Xu, W. and Hu, H. (2021): Penetration of annular and general jets into underwater plates. Computational Particle Mechanics, 8(2), 289–296. https://doi.org/10.1007/s40571-020-00330-9

Liu, G.R. and Liu, M.B. (2003): Smoothed Particle Hydrodynamics; A Meshfree Particle Method; World Scientific: London, UK.

Baranowski, P., Małachowski, J. and Mazurkiewicz, Ł. (2020): Local blast wave interaction with tire structure. Defence Technology, 16(3), 520–529. https://doi.org/10.1016/j.dt.2019.07.021

Panowicz, R. and Konarzewski, M. (2020): Influence of imperfect position of a striker and input bar on wave propagation in a split Hopkinson pressure bar (SHPB) setup with a pulse-shape technique. Applied Sciences (Switzerland), 10(7). https://doi.org/10.3390/app10072423

Kurzawa, A., Pyka, D., Jamroziak, K., Bocian, M., Kotowski, P. and Widomski, P. (2018): Analysis of ballistic resistance of composites based on EN AC-44200 aluminum alloy reinforced with Al2O3 particles. Composite Structures, 201, 834–844. https://doi.org/10.1016/j.compstruct.2018.06.099

Xu, W., Wang, C. and Chen, D. (2019): Formation of a borecenter annular shaped charge and its penetration into steel targets. International Journal of Impact Engineering, 127, 122–134. https://doi.org/10.1016/j.ijimpeng.2019.01.008

Sliwinski, J., Ludas, M., Kosnik, S., Pyka, D. and Jamroziak, K (2016): Investigations of the Detonation Wave Propagation Process in the ŁK Cumulative Charge; Research report; Ammunition Testing Laboratory: Wroclaw, Poland, Unpublished materials.

Mehreganian, N., Louca, L. A., Langdon, G. S., Curry, R. J. and Abdul-Karim, N. (2018): The response of mild steel and armour steel plates to localised air-blast loading-comparison of numerical modelling techniques. International Journal of Impact Engineering, 115, 81–93. https://doi.org/10.1016/j.ijimpeng.2018.01.010

Nsiampa, N., Coghe, F. and Dyckmans, G. (2009): Numerical investigation of the bodywork effect (K-effect). May, 1561–1566. https://doi.org/10.1051/dymat/2009220

SAŽETAK

Numerička optimizacija EFP naboja temeljena na MPB mini

U članku je prikazana numerička optimizacija eksplozivno formiranoga umetka punjenja na bazi protumetka, protutenkovske MPB mine. U tu svrhu, prije svega, analizirani su kemijski sastav i mikrostruktura trenutačno korištenih EFP umetaka i ciljnoga materijala – oklopnoga čelika. Potom je proveden niz numeričkih analiza tijekom kojih je promijenjen ne samo materijal EFP umetka, već i njegova debljina, u smislu najučinkovitije kombinacije, odnosno početne brzine pri oblikovanju, ali i probojne sposobnosti umetka. Johnson-Cookov model konstitutivne čvrstoće korišten je za opisivanje ponašanja materijala u računalnome okruženju, a Jones-Wilkins-Leejev model korišten je za opisivanje tlaka tijekom detonacije. Za opis nastanka EFP naboja korištena je hidrodinamika SPH čestica koju je autor razvio u svojim prethodnim radovima, zahvaljujući kojoj je bilo moguće učinkovito opisati visokodinamički proces. Posljednji element istraživanja bila je validacija numeričkih modela provedenih na vojnome poligonu tijekom eksperimentalne studije. Rezultati numeričkih analiza omogućili su određivanje optimalne kombinacije materijala i debljine umetka, što je uputilo na buduće smjerove razvoja u cilju poboljšanja rješenja u području protutenkovskoga EFP-a.

Ključne riječi:
protutenkovske mine izvan rute, eksplozivni projektil, fenomen velike brzine, hibridne numeričke metode, metoda konačnih elemenata

Author's contribution

Dariusz Pyka: conceptualization, reserch, writing, editing.